Blind deconvolution of turbulence-degraded images using natural PSF priors

Roberto Baena Gallé[1,2,3], Szymon Gladysz[3], Laurent Mugnier[4], Rao Gudimetla[5], Robert L. Johnson[5], Lee Kann[5]

[1]*University of Barcelona, c\Marti I Franqués 1, 08025 Barcelona, Spain*
[2]*Royal Academy of Sciences and Arts of Barcelona, Rambla dels Estudis 115, 08002 Barcelona, Spain*
[3]*Fraunhofer Institute of Optronics, System Technologies and Image Exploitation, Gutleuthausstr. 1, 76275 Ettlingen, Germany*
[4] *ONERA/DOTA (Département d'Optique Théorique et Appliquée), B.P. 72, 92322 Châtillon cedex, France*
[5]*Air Force Research Laboratory, Directed Energy Directorate, Kirtland AFB, NM, USA*

Author e-mail address: rbaena@am.ub.es

Abstract: Deconvolution of images taken through atmospheric turbulence often requires regularization in order to prevent the restoration algorithm over-fitting the noisy observation. For this purpose many *object* priors have been proposed but their utility might be limited to one class of real objects. Optical effects of atmospheric turbulence are well understood and therefore priors on the *point-spread function* form a viable alternative. We show their usefulness.
OCIS codes: (110.0115) Imaging through turbulent media, (100.1455) Blind deconvolution

1. Introduction

Solutions to recovery of high-resolution images when observing through atmospheric turbulence usually fall into the software ("post-processing") or the hardware (adaptive optics, interferometry) category or the combination of both. Even with very expensive adaptive optics (AO) systems it is necessary to use deconvolution (image reconstruction) to remove image blurring completely [1,2].

Successful restoration of images degraded by atmospheric turbulence was first achieved using the so-called speckle imaging techniques [3]. Speckle imaging works because average short-exposure power spectrum has non-negligible spectral content up to the telescope's diffraction limit D/λ [4]. On the other hand, for long exposures average optical transfer function (OTF) quickly drops to values below the noise limit above the cut-off r_0/λ. No information can be recovered from the part of the spectrum where signal-to-noise ratio (SNR) falls below unity. It is this SNR cutoff that actually determines available resolution, with or without deconvolution, and the SNR cutoff is nearly always short of the diffraction cutoff [5]. Therefore, non-regularized deconvolution of long-exposure images, taken without AO, rarely results in reliable amplification of the high-frequency content.

Multi-frame blind deconvolution (MFBD) [6-8] is an image reconstruction method relying on the availability of several images of an object. In addition, many of the MFBD algorithms rely on short exposures for the reason stated above. The multiplicity of image frames acts as an implied constraint because the object is common to every image, while noise and turbulence fluctuations vary randomly between frames [5]. Even with this advantage, MFBD can get easily trapped in local minima [9]. We are studying approaches to alleviating this problem.

2. Motivation

Regularization is the most popular approach to balancing resolution enhancement and amplification of noise. We include statistical prior information through the maximum *a posteriori* (MAP) approach. There, one finds estimates for the object **o** and the PSFs **h** which jointly maximize the expression:

$$[\hat{\mathbf{o}},\hat{\mathbf{h}}] = \arg\max_{\mathbf{o},\,\mathbf{h}} p(\mathbf{o},\mathbf{h}|\,\mathbf{i}) = \arg\max_{\mathbf{o},\,\mathbf{h}} p(\mathbf{i}|\,\mathbf{o},\mathbf{h}) \times p(\mathbf{o}) \times p(\mathbf{h}) \tag{1}$$

where **i** is the data. Historically, most efforts were directed towards finding useful expressions for the prior probability of the object, $p(\mathbf{o})$. Since actual probability density function (PDF) of the object is in general not known, solutions in the form of functions with desirable mathematical properties (e.g. noise suppression, edge enhancement) are often used. As these *ad hoc* formulas are not real PDFs, regularization parameters must be used to balance their influence on the cost function in Equation (1). Often these parameters have to be chosen manually [1,8]. Apart from the problem of choosing the right value for them, the mere form of the prior (e.g. an object's power spectral density) could be applicable only to a limited class of real objects, although the object's power spectral density could be estimated from the images themselves [10]. In this paper we focus on PSF priors because for the problem treated here – imaging through Kolmogorov turbulence – they will be generally applicable to all objects being imaged. As such, they hold the promise of eliminating the need for regularization parameters. We are testing this hypothesis.

3. Methodology

For the data-fidelity term in Equation (1) we use the standard maximum-likelihood expression under the assumption of stationary Gaussian noise. For the PSF constraint we use image intensity statistics although constraints in other domains (pupil-plane or Fourier-frequency) are also possible [11]. Our goal is to make blind deconvolution automatic, or at least less user-dependent than it currently is (the "art" of deconvolution). Therefore we strived to find approaches capable of extracting the (average) PSF directly from the data. For this purpose we use the "Fourier contrast" method [12]. It should be noted that this average PSF is also required for computation of the prior probability of each of the PSFs, $p(\mathbf{h})$, in our multi-frame algorithm.

To model short-exposure PSF statistics use is made of the gamma PDF [4]:

$$p(\mathbf{h}) = \prod_{k}^{K} \prod_{x}^{X} \prod_{y}^{Y} \frac{1}{\Gamma(M)} \left(\frac{M}{\langle \mathbf{h}(x,y) \rangle} \right)^{M} \mathbf{h}(k,x,y)^{(M-1)} \exp\left\{ -\frac{M\,\mathbf{h}(k,x,y)}{\langle \mathbf{h}(x,y) \rangle} \right\} \tag{2}$$

where K is the number of speckle frames and X and Y are the numbers of pixels in x and y directions, M is the general integration parameter, a product of the spatial, spectral and temporal integration parameters [13]. This PDF was tested on simulated data with good results [14]. The PDFs were converted to negative log-likelihoods and, together with analytic gradients, inserted into a Variable Metric with Limited Memory (VMLM) optimizer [15].

An alternating approach is used to jointly calculate both the object and the PSFs. In this approach, the object is first estimated with the current set of PSFs. After ten VMLM iterations, the current estimate of the object is used to update each PSF in ten new VMLM iterations. This double process constitutes one iteration of the main loop. Subsequently, the updated set of PSFs is used to re-estimate the object thus starting a new loop. The algorithm is stopped after a user-specified number of iterations or after the object achieves some level of convergence. For the results shown in this paper, we forced convergence level to be very demanding and so the maximum number of iterations was always reached first.

The VMLM object-loop can be replaced by the Wiener filter estimation [16]. This object estimate is then used to update the PSFs. This allows us to reduce the computation time because ten iterations of the non-linear VMLM process are substituted by only one Wiener-filter operation. Besides, it also allows us to introduce some prior knowledge about the object by means of its power spectral density [17].

4. Input data

I-band (800-900 nm) observations of the bright single star HR2219 have been obtained with the 3.5 m telescope at the Starfire Optical Range with adaptive optics switched off (but with the tip/tilt system switched on). Thousand frames were recorded, with exposure time set to 10 ms. We obtained $D/r_0 = 34$ (and so $r_0 = 10.5$ cm) from the Fourier contrast method. Speckle images from HR2219 were used as PSFs. They were convolved with a schematic representation of the Hubble Space Telescope (Figure 1) which acted as the true object. The resulting images were corrupted with Gaussian noise of standard deviation equal to 1 count. This corresponds to signal-to-noise ratio of around one hundred in the blurred data (Figure 1).

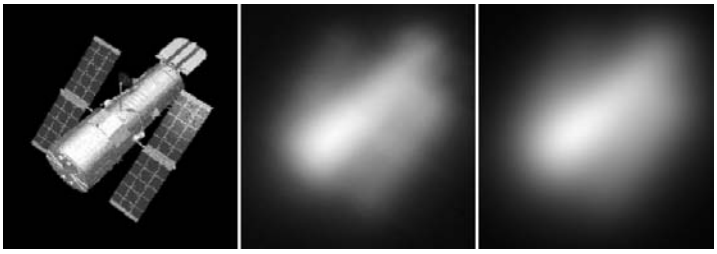

Fig. 1. Left: original object. Center: arbitrarily chosen short-exposure image. Right: long-exposure image. Images are represented in individual min-max scales.

5. Results

Figure 2 shows visually the benefit of using PSF prior in terms of delaying the onset of noise amplification. This figure is based on tests with 100 frames whereby the average PSF was computed directly from the data. To quantify reconstruction quality we used the peak signal-to-noise ratio (PSNR) [14]. When examining the plots in Figure 3 (left) the reader should remember that PSNR is a logarithmic metric. Here, we supplied the algorithm with initial

PSFs which were the original star images used to produce the input data but additionally blurred with Gaussian functions.

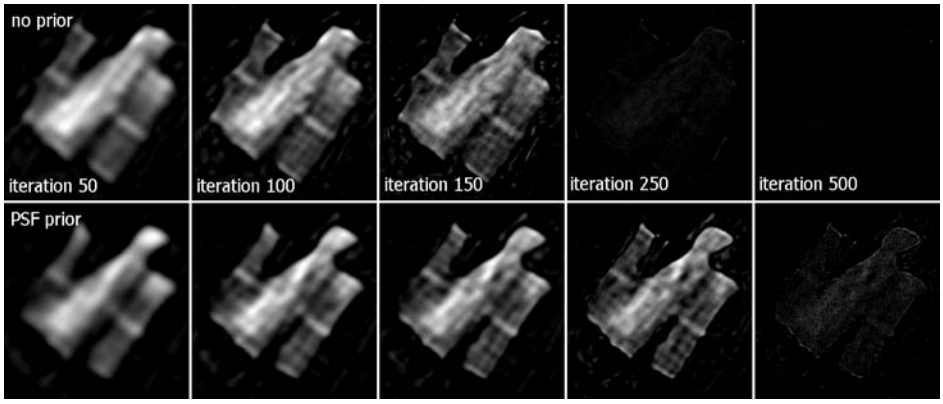

Fig. 2. Top: results at various stages of the reconstruction process based on data-fidelity term alone. Bottom: results with the PSF prior. Images are represented in individual min-max scales. Initial PSF: Fried's model based on r_0 = 10.5 cm from the Fourier contrast method [12].

We also tested the susceptibility of the blind reconstruction process to initial (average) PSF guess. It turns out that deconvolution is actually very susceptible to the starting point (Figure 3, right). Actual *blind* deconvolution would have little chance of producing the desirable output.

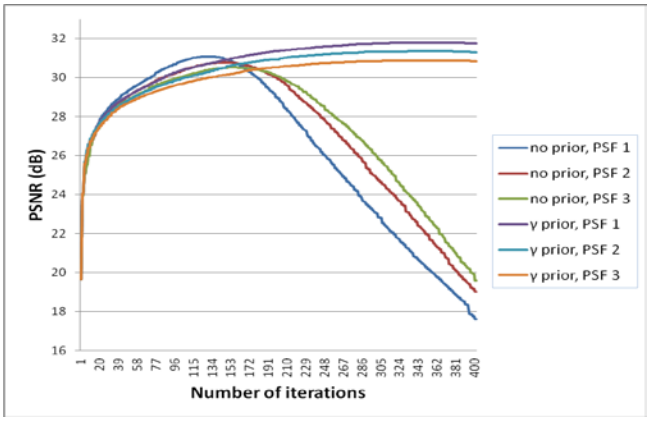

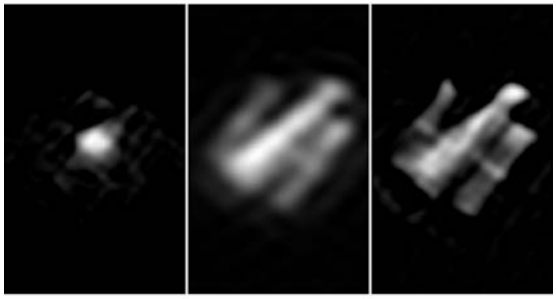

Fig. 3. Left: evolution of the PSNR metric for the tests with and without PSF prior, based on 25 frames. Initial PSF: three different blurred versions of the real kernel used to create the dataset. Right: reconstruction results at 50th iteration when the algorithm was supplied with mismatched PSF based on r_0 = 5 cm (left panel) and r_0 = 15 cm (middle panel). Also shown is the reconstruction obtained with correct r_0 = 10.5 cm (right panel). In all three cases initial PSF was a synthetic one based on the Fried's model from the Fourier contrast method.

ACKNOWLEDGEMENTS: Effort sponsored by U.S. Air Force Office of Scientific Research, Air Force Material Command, under grant FA8655-12-1-2115, and the Spanish Ministry of Science under grant AyA2008-01225. The U.S. Government is authorized to reproduce and distribute reprints for Governmental purpose notwithstanding any copyright notation thereon.

5. References

[1] L. M. Mugnier, T. Fusco, and J.-M. Conan, "MISTRAL: a myopic edge-preserving image restoration method, with application to astronomical adaptive-optics-corrected long-exposure images," J. Opt. Soc. Am. A 21, 1841-1854 (2004).
[2] R. Baena Gallé, J. Núñez, and S. Gladysz, "Extended object reconstruction in adaptive-optics imaging: the multiresolution approach," submitted to Astronomy & Astrophysics.
[3] A. Labeyrie, "Attainment of diffraction-limited resolution in large telescopes by Fourier-analyzing speckle patterns in star images," Astronomy & Astrophysics 6, 85-87 (1970).
[4] J. W. Goodman, "Speckle phenomena in optics: theory and applications," (Roberts & Company, 2006).
[5] D. W. Tyler, "Deconvolution of adaptive optics image data," Proceedings of the Center for Adaptive Optics, (2001).
[6] T. J. Schulz, "Multiframe blind deconvolution of astronomical images," J. Opt. Soc. Am. A 10, 1064-1073 (1993).
[7] D. G. Sheppard, B. R. Hunt, and M. W. Marcellin, "Iterative multiframe superresolution algorithms for atmospheric-turbulence-degraded imagery," J. Opt. Soc. Am. A 15, 978-992 (1998).
[8] C. L. Matson, K. Borelli, S. Jefferies, C. C. Beckner, Jr., E. K. Hege, and M. Lloyd-Hart, "Fast and optimal multiframe blind deconvolution algorithm for high-resolution ground-based imaging of space objects," Appl. Opt. 48, A75-A92 (2009).
[9] J. Nagy and V. Mejia-Bustamante, "MFBD and the local minimum trap," Proceedings of the AMOS Conference, 2009, Ed.: S. Ryan, The Maui Economic Development Board, p.E10
[10] L. Blanco and L. M. Mugnier, "Marginal blind deconvolution of adaptive optics retinal images," Opt. Express 19, 23227-23239 (2011).
[11] R. Baena Gallé, S. Gladysz, L. Mugnier, R. Gudimetla, R. Johnson, and L. Kann, "Physically-constrained Multi-frame Blind Deconvolution," in Adaptive Optics: Methods, Analysis and Applications, The Optical Society, 2013
[12] S. Gladysz, R. Baena Gallé, R. Johnson, and L. Kann, "Image reconstruction of extended objects: demonstration with the Starfire Optical Range 3.5m telescope," Proceedings of SPIE, Volume 8535, 85350M-1-13 (2012).
[13] S. E. Skipetrov, J. Peuser, R. Cerbino, P. Zakharov, B. Weber, and F. Scheffold, "Noise in laser speckle correlation and imaging techniques," Opt. Express 18, 14519-14534 (2010).
[14] R. Baena Gallé, S. Gladysz, L. Mugnier, R. Gudimetla, R. Johnson, and L. Kann, "Unsupervised blind deconvolution," Proceedings of the AMOS Technical Conference, Maui, 10-13 September 2013, p. E20
[15] E. Thiebaut, "Optimization issues in blind deconvolution algorithms," in Astronomical Data Analysis II, SPIE Vol. 4847, 174-183 (2002).
[16] D. R. Gerwe, M. Jain, B. Calef, and C. Luna, "Regularization for nonlinear image restoration using a prior on the object power spectrum," Proc. SPIE 5896, 1-15 (2005).
[17] J-M. Conan, L. Mugnier, T. Fusco, V. Michau, and G. Rousset, "Myopic deconvolution of AO images by use of object and PSF power spectra, " Applied Optics 37, 4614-4621 (1998).